

## THE MAGNETIC FUTURE OF THE SUN

PHILIP G. JUDGE<sup>1</sup>, RICKY EGELAND,<sup>1</sup> TRAVIS S. METCALFE,<sup>2</sup> AND EDWARD GUINAN,<sup>3</sup> SCOTT ENGEL<sup>3</sup>

<sup>1</sup>*High Altitude Observatory, National Center for Atmospheric Research<sup>a</sup>, P.O. Box 3000, Boulder CO 80307-3000, USA*

<sup>2</sup>*Space Science Institute, 4750 Walnut Street, Suite 205, Boulder CO 80301, USA*

<sup>3</sup>*Astronomy and Astrophysics Department, Villanova University, 800 Lancaster Ave, Villanova PA 19085, USA*

### ABSTRACT

We analyze space- and ground-based data for the old ( $7.0 \pm 0.3$  Gyr) solar analogs 16 Cyg A and B. The stars were observed with the Cosmic Origins UV Spectrographs on the Hubble Space Telescope (HST) on 23 October 2015 and 3 February 2016 respectively, and with the Chandra X-ray Observatory on 7 February 2016. Time-series data in Ca II data are used to place the UV data in context. The UV spectra of 18 Sco ( $3.7 \pm 0.5$  Gyr), the Sun ( $4.6 \pm 0.04$  Gyr) and  $\alpha$  Cen A ( $5.4_{-0.2}^{+1.2}$  Gyr), appear remarkably similar, pointing to a convergence of magnetic heating rates for G2 main-sequence stars older than  $\approx 2 - 4$  Gyr. But the B component's X-ray (0.3-2.5 keV) flux lies  $20\times$  below a well-known minimum level reported by Schmitt. As reported for  $\alpha$  Cen A, the coronal temperature probably lies below that detectable in soft X-rays. No solar UV flux spectra of comparable resolution to stellar data exist, but they are badly needed for comparison with stellar data. Center-to-limb (C-L) variations are re-evaluated for lines such as Ca II through to X-rays, with important consequences for observing activity cycles in such features. We also call into question work that has mixed solar intensity-intensity statistics with flux-flux relations of stars.

*Keywords:* stars: individual – stars: activity – stars: chromospheres – stars: coronae

arXiv:1710.05088v1 [astro-ph.SR] 13 Oct 2017

<sup>a</sup> The National Center for Atmospheric Research is sponsored by the National Science Foundation

## 1. INTRODUCTION

Ultraviolet emission from the Sun was originally inferred by the existence of the ionosphere (e.g. Chapman 1931; Woolley & Allen 1948). Solar UV radiation arises primarily because mechanical energy from the solar interior is deposited into the Sun’s tenuous atmosphere, in structures from which UV photons can escape. Solar observations from the space era reveal clear evidence that the solar magnetic field is the agent responsible for heating most of the plasma capable of emitting UV photons that can escape and reach the Earth (as reviewed by Eddy 2009).

Solar magnetism exhibits remarkable properties. The Sun acts as a magnetic machine. A small fraction of the energy from nuclear fusion is partitioned into magnetic energy, which is manifested in two seemingly universal phenomena entirely unanticipated from first principles (e.g. Judge 2017). Firstly, it regenerates its entire magnetic field every 22 years, and secondly, it converts a small but (for life on Earth) significant amount of energy into high energy photons and particles flooding the solar system.

We have yet to find a Sun-like star that does not emit soft X-rays (Schmitt 1997). The Sun’s outer layers, sitting atop an atmosphere with energies close to 0.4 eV (4500 K), appear to emit UV radiation (10 eV), X-rays (100-5000 eV), even occasionally  $\gamma$ -rays (MeV) during flares. The varying magnetic field in Sun-like stars produces near-UV emission in the cores of Fraunhofer’s *H* and *K* lines of Ca II (Leighton 1959; Linsky & Avrett 1970). Such changes, readily observable from the ground, have been cataloged for more than 5 decades (Wilson 1968, 1976; Baliunas et al. 1995; Hall & Lockwood 2004; Hall et al. 2009; Egeland et al. 2017). Examples of this behavior for 18 Sco, 16 Cyg A and B, are shown in Figure 1. The Sun-as-a-star shows modest variations in the *H* and *K* lines, somewhat less than the variations shown for 18 Sco (Egeland et al. 2017). All such variations are clearly associated with surface magnetism (Skumanich et al. 1975). These and other observations indicate that the Sun is not alone in showing its magnetic fingerprints, decadal variations are common amongst late-type stars on the main-sequence (Baliunas et al. 1995). Here we study new UV line profiles for two optically “bright” stars that are older than the Sun, 16 Cyg A and B, obtained with the Cosmic Origins Spectrograph (COS) on the Hubble Space Telescope (HST). These stars are among the weakest activity main-sequence sun-like stars found. Earlier generations of UV spectrographs were not sensitive enough to obtain useful data. The FUSE spacecraft did detect EUV emission lines (C III 977, O VI 1031) in the A component,

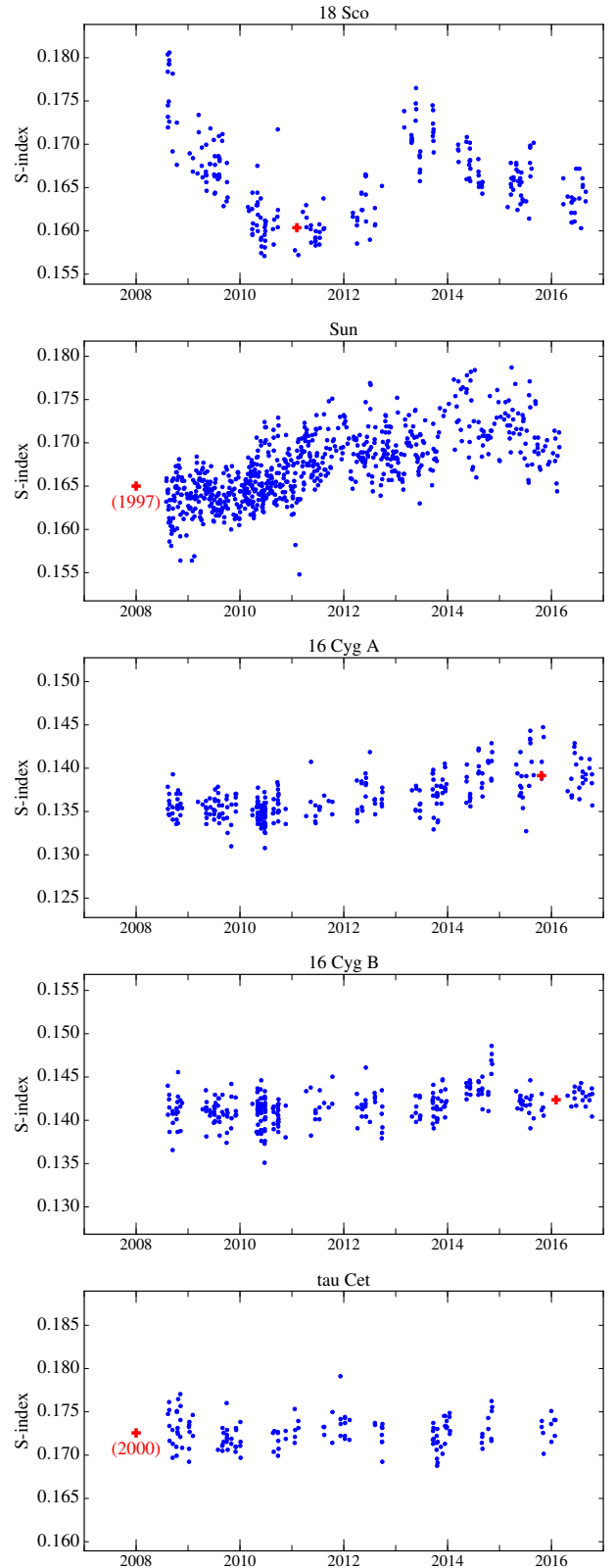


**Figure 1.** Solar Stellar Spectrograph *S*-index data for 18 Sco, the Sun, 16 Cyg A and B and  $\tau$  Cet are shown, from Egeland et al. (2017). Each plot spans a range of 0.035 in *S*, so that amplitudes can be directly compared. Red crosses mark the time of the COS UV stellar observations and the 2-year *S*-index median centered at that time. The solar UV data were obtained close to solar minimum on April 20, 1997. STIS data for  $\tau$  Cet were obtained on August 1 2000. These two data points are arbitrarily plotted at year 2008.

but the S/N ratios were insufficient to probe properties of line profiles (Guinan et al. 2003) that dynamically reflect magnetic field activity in the atmospheres of stars and the Sun.

Our main purpose here is to study properties of the UV emission lines (formed between  $\approx 8000$  to  $200,000$  K) with age, extending previous studies of bright young targets to relatively dim and old stars in the 16 Cygni system. The emission features of doubly- and triply-charged ions in Sun-like stars reflect magnetic heating mechanisms through their mere presence (Athay & White 1978, 1979). Hydrodynamic processes alone also fail to account for even the most basic properties of line profiles of the “chromospheric” C II 133.5 nm multiplet (Judge et al. 2003a). X-ray studies show that coronae are present on all Sun-like stars in a volume limited sample (Schmitt 1997). Coronae must be powered by magnetic fields emerging from beneath the stellar surfaces, as must the broad line components observed in  $\alpha$  Cen A and the Sun. Specifically, we study the Ca II  $S$ -index time series, the UV line profiles from the Hubble Space telescope, including both core and broad components, as well as available X-ray data.

The most striking feature we find, is the remarkable similarity in the UV spectra of all the G2 stars. We show that this agreement is, at first inspection, quite “unreasonable”, given what we know of stellar flux-flux relationships and the known variations of the Ca II  $S$ -indices for these stars. A resolution of this difficulty is proposed. We speculate on implications for the future surface magnetism of the Sun and other G-type stars for the latter portions of their main sequence lifetimes.

## 2. ANALYSIS

Table 1 lists basic data for the Sun and five stars analyzed here. The age of  $\tau$  Cet is near 7.6 Gyr, but its lower mass of  $0.78 M_{\odot}$ , separates it from the other Sun-like stars discussed below. We included the star because so few HST spectra of old GV stars exist, and it has been discussed as a proxy for the Sun in a grand minimum state (Judge et al. 2004).

### 2.1. New observations

COS observations were acquired under program 13861 (E. Guinan, P.I.). The circumstances of these observations are given in Table 2 and these epochs are marked in Figure 1. These data were processed using Version 3.3 of the IDL procedure COADD\_X1D<sup>1</sup> using default parameters. We used HST data for stars other than these and 18 Sco, processed and described by Judge et al.

(2004). G130M Data for 18 Sco were downloaded from the MAST archive and processed as for the 16 Cygni stars. No G160M or other moderate resolution HST data exist for 18 Sco. The 18 Sco COS spectra used here are from program 12303 (E. Guinan, P.I., see Table 2). The absolute flux calibration of the HST UV spectrographs is known to better than 5% (Pagano et al. 2015). For later reference, the flux calibration for low resolution (6Å) spectra from the International Ultraviolet Explorer is  $\leq 10\%$  (González-Riestra et al. 2001).

### 2.2. The HST data in the context of magnetic variations

In Figure 1 time-series of the Ca II “ $S$ -index” for the 16 Cyg stars and 18 Sco, are marked with the epochs of the observations with COS. The solar data are shown for the same period, also showing the  $S$ -index when the partial-disk observations were acquired (April 1997, Curdt et al. 2001). The solar data are from a typical region, averaging data from along SUMER’s  $1 \times 300''$  slit. This region samples just 0.01% of the solar area, extending over a region covering  $\cos \vartheta \approx 1$  to 0.988, where  $\vartheta$  is the angle between local vertical on the Sun and line-of-sight.

We emphasize that the solar data shown are *intensity* data, i.e. from a small, resolved part of the solar disk. The stellar data are *flux* spectra. *A high resolution UV flux spectrum of the Sun does not exist.* These differences will be important below.

The Ca II data in Figure 1 were obtained from the Lowell Observatory Solar-Stellar Spectrograph from 2008 to 2016, following an upgrade of the instrument CCD detector. The instrument and data reduction are described by Hall et al. (2007) with updates in Egeland et al. (2017). The data were calibrated to the Mount Wilson Observatory instrumental scale using near-coincident measurements, as described in Egeland (2017). The “ $S$ -index” measures the brightness of the chromospheric cores of the Ca II resonance lines relative to the neighboring line wings (e.g. Wilson 1968; Vaughan et al. 1978). Ca II core emission is a well-known “proxy” for the amount of magnetic activity in late-type stars (Leighton 1959; Skumanich et al. 1975). From Figure 1, it is clear that 18 Sco was observed with COS close to a minimum in  $S$ -index. The 16 Cyg stars have no clear cycle such as that seen in 18 Sco with a period close to 7 years, or the Sun with a period close to 11 years. The solar measurements are also from a period close to a minimum  $S$ -index, but these measurements are from quiet regions close to disk-center only.

Figure 2 summarizes long-term variability in the  $S$ -index shown in Figure 1. The range of  $S$ -index vari-

<sup>1</sup> <http://casa.colorado.edu/home/~danforth/science/cos/>

**Table 1.** Fundamental data for older main sequence stars

Star	Sp type	Age (Gyr)	$M$ ( $M_{\odot}$ )	$R$ ( $R_{\odot}$ )	$L^{\dagger}$ ( $L_{\odot}$ )	$P_{\text{rot}}$ (days)	R.V. ( $\text{km s}^{-1}$ )	$\phi'$ (mas)
18 Sco	G2 V	$3.7 \pm 0.5^a$	$1.03 \pm 0.01^a$	$1.01^b$	1.06	$22.7^c$	+11.6	$0.6797 \pm 0.0062$
Sun	G2 V	$4.6 \pm 0.04^d$	1	1	1	25.4	0	...
$\alpha$ Cen A	G2 V	$5.4^{+1.2}_{-0.2}^e$	$1.11 \pm 0.01^e$	$1.227^f$	1.53	$22\text{--}29^g$	−23.45	$8.662 \pm 0.02$
16 Cyg A	G1.5 Vb	$7.0 \pm 0.3^h$	$1.08 \pm 0.02^h$	$1.194^i$	1.58	$23.8^j$	−27.5	$0.539 \pm 0.007$
16 Cyg B	G3 V	$7.0 \pm 0.3^h$	$1.04 \pm 0.02^h$	$1.108^i$	1.24	$23.2^j$	−28.1	$0.481 \pm 0.006$
$\tau$ Ceti	G8 V	$7.6^{+0.9}_{-1.5}^k$	$0.78 \pm 0.01^l$	$0.793^l$	0.50	$34^m$	$-16.4 \pm 0.9$	$2.03 \pm 0.05$

NOTE—Spectral types and radial velocities (R.V.) are from the SIMBAD database.  $\dagger$  Luminosities are from Valenti & Fischer (2005). References: <sup>a</sup>Li et al. (2012), <sup>b</sup>Bazot et al. (2011), <sup>c</sup>Petit et al. (2008), <sup>d</sup>Houdek & Gough (2011), <sup>e</sup>Bazot et al. (2016), <sup>f</sup>Kervella et al. (2003), <sup>g</sup>Mamajek & Hillenbrand (2008), <sup>h</sup>Metcalfe et al. (2015), <sup>i</sup>Adopted from seismic data of Buldgen et al. (2016), supported by interferometric work of White et al. (2013) who found radii of  $1.22 \pm 0.02$  and  $1.12 \pm 0.02 R_{\odot}$  for 16 Cyg A and B respectively. <sup>j</sup>Davies et al. (2015), <sup>k</sup>Pagano et al. (2015), <sup>l</sup>Tang & Gai (2011), <sup>m</sup>Baliunas et al. (1996). The angular diameters  $\phi'$  were derived from *Hipparcos* distances and listed radii.

**Table 2.** Stellar data from HST/COS

Target	COS Grating <sup>†</sup>	Start Time UTC	Exposure sec	$\lambda$ range nm
18 Sco	G130M	2011-02-04 21:46	2700.54	115-145
16 Cyg A	G130M	2015-10-23 01:58	11677.8	115-145
	G160M	2015-10-23 08:21	5882.6	140.5-177.5
16 Cyg B	G130M	2016-02-03 01:10	11674.5	115-145
	G160M	2016-02-03 07:31	5882.4	140.5-177.5

NOTE—16 Cyg data are from program 13861. 18 Sco data are from program 12303. <sup>†</sup>The observation IDs are LCN501010 (for G130M) and LCN501020 (G160M) for the 16 Cyg stars, and LBIZ01020 for 18 Sco.

ability decreases with age, as can be seen by the spread in the seasonal mean values as well as the interquartile range. The Sun’s larger total range may be enhanced by the significantly higher sampling cadence. Using the more robust seasonal medians and interquartile range, the younger 18 Sco varies by a few percent more than the Sun, while the older stars 16 Cyg A and B vary a few percent less. The flat activity star  $\tau$  Ceti, also of significantly lower mass, has the smallest range of

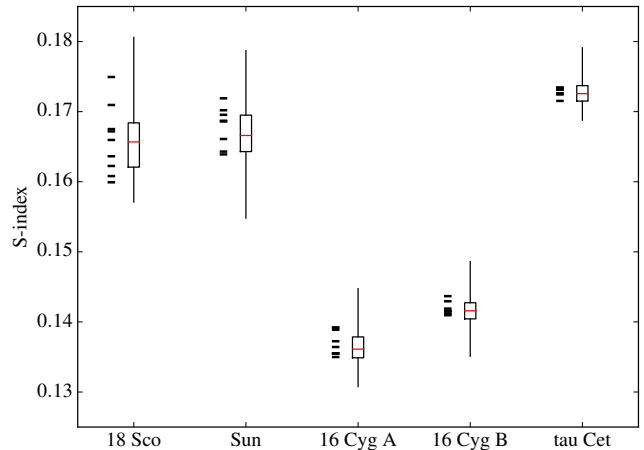


**Figure 2.** Solar Stellar Spectrograph  $S$ -index variability from 2008 to 2016. The stars are listed in order of increasing age. Black dashes show seasonally binned medians, or 1-year binned medians for the Sun. The box extends from the lower to upper quartile values of the data, with a line at the median. The whiskers extend from the box to show the total range of the data. The boxes span a range in  $S$ -index equivalent to  $1.47\sigma$ , where  $\sigma$  is the width parameter in a normal distribution.

variability of the sample. Indeed, this star might be in a state analogous to the solar “Maunder Minimum”, a period of temporarily reduced spot activity during a longer phase of cyclic variations (e.g. Judge et al. 2004). Alternatively, it could be in a permanent state of mag-

netic quiescence brought about by a reconfiguration of the large-scale field (Metcalf et al. 2016), which may occur in all middle-aged sun-like stars (van Saders et al. 2016). Interestingly, with spectral type G8 V,  $\tau$  Cet is almost a K star. Main sequence K stars are highly likely to be found exhibiting cycling behavior (Egeland 2017).

### 2.3. Differential comparison of five stars

Pertinent emission features in the spectra of these stars are shown in Figure 3. The figure shows the surface flux density  $\mathcal{F}_\lambda = 1.70 \times 10^{17}/(\phi')^2 f_\lambda$ , where  $f_\lambda$  is the flux density measured at Earth. The Figure includes lines formed mostly in the solar transition region: Si III 120.6 nm, N V 124.2 nm, Si IV 139.3 and 140.2 nm, C IV 154.8 and 155.0 nm. The O V] at 121.8 nm is also present, but shown in Figure 6. Lines of neutral carbon near 165.7 nm are highlighted, along with the multiplet of C II at 133.4 and 133.5 nm. Other lines of H I  $L\alpha$  (121.5 nm) and O I (130.2, 130.4, 130.6, 135.6, 135.9 nm) are contaminated by emission from the Earth’s geo-corona, or are rather weak (N I 131.9 nm). The panel labeled “O V]” in Figure 3 contains broad emission in the wing of H I  $L\alpha$  121.5 nm, with significant contamination from the geocorona in the COS data shown.

We consider first the four G1 to G3 V stars as a group, excluding the Sun, for which no comparable flux spectrum exists. Remarkably, the flux spectra (i.e. spectra other than those of the Sun itself) are *qualitatively and qualitatively very similar*. Let us consider the lines in terms of increasing temperature of formation. The purely chromospheric C I 165.7 nm flux densities are within 10 percent of one another. The C II multiplet ( $2s^2 2p \ ^2P^\circ \ 2s 2p^2 \ ^2D$ ) consists of three transitions, the  $J = 1/2 \rightarrow J' = 3/2$  line at 133.4532 nm, and the  $J = 3/2 \rightarrow J' = 3/2, 5/2$  blended lines at 133.5663 and 133.5778 nm. The blended 133.57 nm profiles are almost identical except in the very cores of the lines. These lines are well resolved spectrally by COS and (for  $\alpha$  Cen A, STIS), as can be seen by the narrow width ( $\approx 0.01$  nm) of the optically thin 135.56 nm chromospheric line of O I] shown in Figure 6.

While the C II 133.45 nm line profiles are affected differently by interstellar absorption, the core flux densities of the 133.56 nm components all lie in the range  $1.3 \pm 0.2 \times 10^5$  ergs cm $^{-2}$  s $^{-1}$  nm $^{-1}$ . All the G2 V stars show small self-reversals in the very core. The profiles of lines of third, fourth and fifth spectra (first spectrum = neutral, second = singly ionized, etc.) all lie within 15% of another. For most lines the  $\alpha$  Cen STIS spectrum is brightest, followed by 18 Sco, 16 Cyg A and 16 Cyg B. Even the 164.0 nm (Balmer- $\alpha$ ) transition of He II, noto-

riously poorly understood, but probably influenced by higher energy photons and/or particles from the corona (Laming & Feldman 1993; Wahlström & Carlsson 1994), varies by less than 15% of the average flux density. The absence of detectable soft X-rays above 0.3 keV found below (section 2.4) does not invalidate the potential role of EUV photons in exciting helium, because helium photoionizations occur for  $\approx 10\times$  softer photons at 0.02 and 0.04 keV for neutral and ionized helium respectively

The 164 and 165 nm regions shown in the figure include some UV continuum which are also remarkably similar in brightness. The UV continuum below 150 nm was shown to be a tracer of magnetic activity and rotation for much younger stars by Linsky et al. 2012. For each of the collisionally-excited transition-region lines in Figure 3 (i.e. except He II and C I), we divided the each flux by the average of the four stellar spectra, and computed the standard deviation of these normalized wavelength-integrated fluxes. The standard deviation is just  $\sigma = 10\%$ .

These results stand in contrast to and strengthen (by extending the sample to older and younger stellar spectra) the differential study of the Sun,  $\alpha$  Cen A (G2 V) and  $\tau$  Cet (G8 V) by Judge et al. (2004). In that work, significant differences were found between the Sun and  $\alpha$  Cen A on the one hand, and the older star  $\tau$  Cet. These differences are evident as  $\tau$  Cet is seen as the low outlier in brightness in the transition region lines in Figure 6, and its lines of Si IV and C IV are systematically blue-shifted relative to the other stars.

### 2.4. Relationship to younger stars

To place these results in a broader context, we searched the list of “solar analog” stars (Table 4.1 of Egeland 2017) for those with useful UV data. The following stars have data from HST or the IUE satellite: HD 20630 ( $P_{\text{rot}} = 9.2$  days,  $L_{\text{BOL}}/L_\odot = 0.82$ ), HD 30495 (11.3, 0.96), HD 72905 (4.89, 0.97), HD 97334 (8.25, 1.06), and HD 76151 (15.0, 0.97). Fundamental data are based upon HIPPARCOS parallaxes and the work of Valenti & Fischer (2005), except for HD72905, where we used Gaidos et al. (2000).

Figure 4 shows scaled flux densities versus age for the old stars together with younger “solar analog” stars with available UV measurements. For each star, a mean value of  $R'_{\text{HK}} = \mathcal{F}_{\text{HK}}/\mathcal{F}_{\text{BOL}}$  is plotted (upper panel), and the equivalent value  $R'_{\text{UV}} = \mathcal{F}_{\text{UV}}/\mathcal{F}_{\text{BOL}}$  is shown in the lower panels for the multiplets of ions of C, Si and He. Here,  $\mathcal{F}_{\text{BOL}} = L_*/4\pi r_*^2$  is the stellar bolometric flux density (erg cm $^{-2}$  s $^{-1}$ ).  $\mathcal{F}_{\text{UV}}$  (also erg cm $^{-2}$  s $^{-1}$ ) is the surface flux density of the line or multiplet, minus the background continuum, integrated over wavelength.



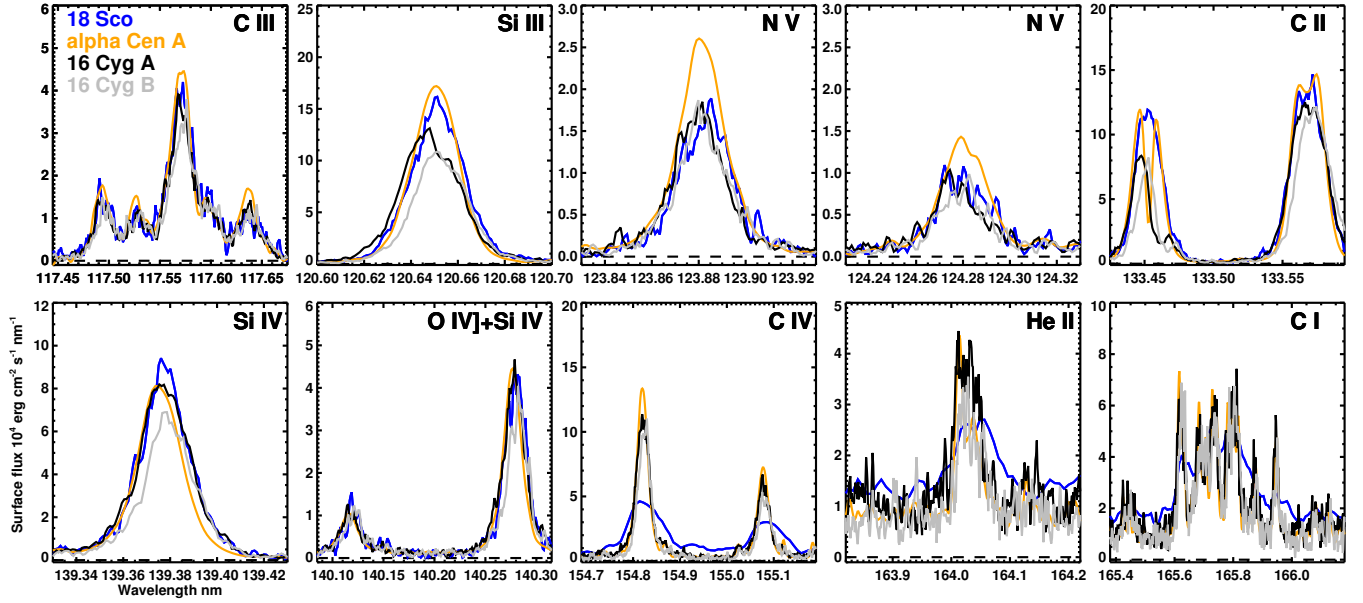


**Figure 3.** Surface flux densities  $\mathcal{F}_{UV}$  of prominent UV lines in the spectra of the stars observed are shown (not including disk-center data for the Sun or  $\tau$  Ceti). The measured flux densities are normalized to unit area of the stellar surface in  $\text{erg cm}^{-2} \text{s}^{-1} \text{nm}^{-1}$ , and the wavelengths have been set to the photospheric reference frame using the relative velocities given in Table 1. The uncertainties in flux density from these HST UV data are  $\pm 5\%$ . Note that data for  $\alpha$  Cen A are from the STIS instrument. Interstellar absorption is present in the 133.45 nm line of C II. In the panel for O V], the “continuum” is a mix of geo-coronal and stellar  $L\alpha$  emission.

Notice the small range in chromospheric  $H$  and  $K$  emission compared with the higher energy UV emission lines. The figure shows a systematic decrease of Ca II and UV  $R'$  values with estimated age. While the  $R'_{HK}$  seems to follow a smooth decline with age, the  $R'_{UV}$  values could also be consistent with a stepwise drop in activity between 2 Gyr and 4 Gyr. It must be noted that the Ca II values for  $R'_{HK}$  are subject to considerable empirical corrections for low-activity stars, because the core emission is weak relative to the bright underlying photospheric component. As is well known, this increase in contrast of UV and X-ray data offer a much cleaner measure of magnetic activity than the Ca II data, at the expense of having to observe from space. Unfortunately, the competition for and relative rarity of satellite UV observations precludes the general use of UV data as proxies of magnetic activity for most stars.

The lowest panel of Fig. 4 shows soft X-ray surface flux densities, again scaled to each target’s bolometric luminosity. The dashed line shows the “minimum” flux density of  $10^4 \text{ erg cm}^{-2} \text{ s}^{-1}$ , found by Schmitt (1997) in the soft ROSAT bandpass, for a star with solar luminosity. Available measures of X-ray activity were obtained as follows: HD 72905 (Ayres 2017); HD 97334 (Linsky et al. 2013); HD 20630 (Ayres 2017); HD 30495 (Wright et al. 2011); HD 76151 (Vidotto et al. 2014); 18 Sco

(DeWarf et al. 2012); a Cen A (Ayres 2017); tau Ceti (Ayres 2017); and the Sun (Ayres 2017).

For 16 Cyg A and B, X-ray activity measures have been acquired by us. In addition to the HST observations of 16 Cyg A and B, contemporaneous X-ray observations were carried out with Chandra on 7 Feb, 2016. Up to that time only upper limits were known. X-ray observations were obtained using the ACIS-I instrument for a total exposure time of 73.9 ksec. The data were reprocessed using CIAO v4.9 and reduced in the usual fashion. X-ray observations were secured for both 16 Cyg A and B, along with 16 Cyg C, the close ( $\approx 3.6''$  separation) M4.5V companion. Despite the long 73.9 ksec exposure time, the total counts for all targets were low. In the ACIS-I energy range of 0.3–2.5 keV, the total counts for 16 Cyg A, B, C are just 43, 3, and 6 respectively, the background noise is  $\approx 1$  count. In order to estimate thermal coronal properties, single temperature MEKAL plasma models (Mewe et al. 1995; Drake et al. 1996) were fitted to the energy distributions using the Sherpa modeling and fitting package, the results are listed in Table 3. The X-ray fluxes of 16 Cyg B more than an order of magnitude below 16 Cyg A. The results for B and C are less secure than for A. For component B it should be considered an upper limit. This upper limit to  $L_X$  lies among the lowest measured so far, for a solar-type star. The modeled temperatures in Table 3

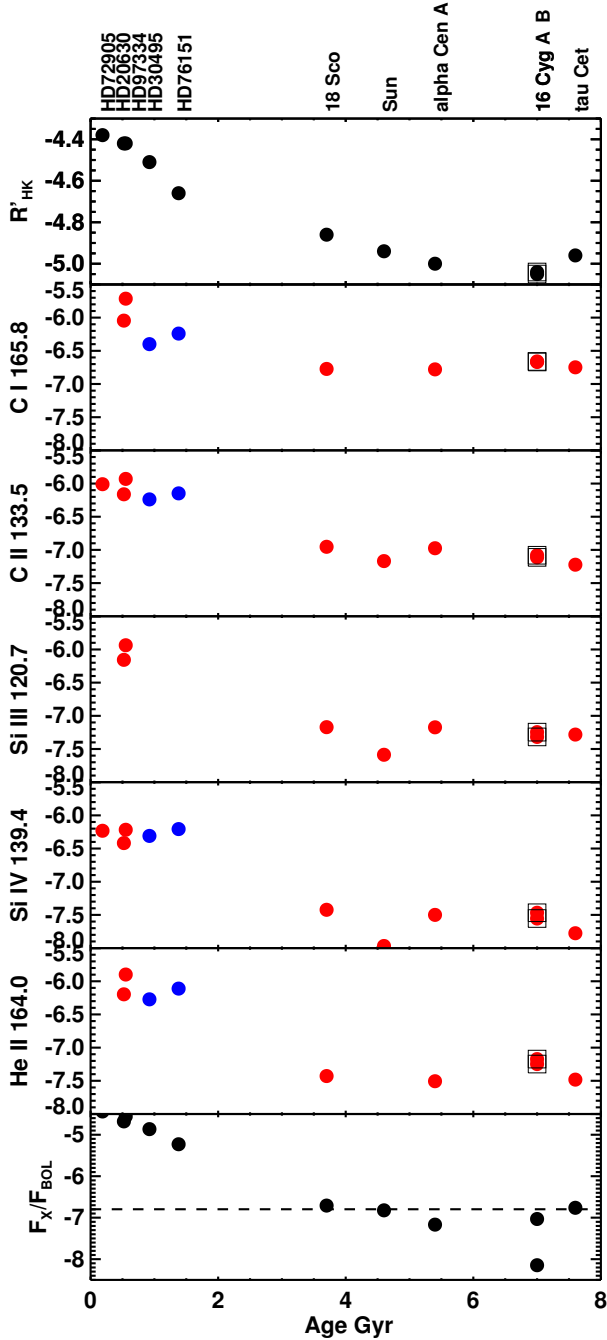


**Figure 4.** Logarithmic flux densities for stars from 0.2 to 7.6 Gyr ages, normalized to the stellar bolometric flux. Blue dots show poorer quality spectra from the IUE satellite, red dots data from the HST. The squares highlight 16 Cyg A and B. The UV solar data plotted show the uncorrected disk center intensities, which are factors  $\beta_i$  below the stellar data owing to the absence of a solar flux spectrum (see text). X-ray data in the lowest panel are from sources in the text. The lowest point is for 16 Cyg B which has  $\log_{10} L_X = 25.5$ . Relative uncertainties are dominated by those in the absolute flux calibrations for the UV lines, at most 14% (IUE vs. IUE), 7% (HST vs. HST) and 11% (IUE vs. HST). 14% corresponds to 0.057 in the logarithm, 2-3 $\times$  smaller than the diameters of the symbols.

**Table 3.** X-ray Parameters of the 16 Cyg ABC System

Star	$kT$ (keV) <sup>a</sup>	$f_X$ (erg s <sup>-1</sup> cm <sup>-2</sup> )	$L_X$ (erg s <sup>-1</sup> )	$\log L_X$ (erg s <sup>-1</sup> )
16 Cyg A	0.37	$1.1 \times 10^{-14}$	$5.7 \times 10^{26}$	26.7
16 Cyg B	...	$\lesssim 6 \times 10^{-16}$	$\lesssim 3 \times 10^{25}$	$\lesssim 25.5$
16 Cyg C	$\approx 0.25$	$\approx 2.6 \times 10^{-15}$	$\approx 1.4 \times 10^{26}$	$\approx 26.1$

In deriving these quantities, We use an interstellar column density  $N_H \approx 4 \times 10^{18} \text{ cm}^{-2}$  from Paresce (1984), with the Hipparcos distance of 21.1 pc.

<sup>a</sup>1 keV  $\equiv 1.2 \times 10^7$  K.

are clearly open to further interpretation. It would help to re-observe this system.

The Ca II time series shown in Figure 1 suggest that the X-ray data were acquired during a season with typical level of chromospheric activity seen on the A and B components since 2008. Also, lines such as N V, generally believed to originate from plasma significantly heated by conduction from the corona, have very similar flux densities in A and B. The remarkably dim X-ray emission of the B component is reminiscent of the behavior of the corona of  $\alpha$  Cen A, found via spectroscopy to be due to a modest cooling of the corona of this star (Ayres et al. 2008). Existing soft X-ray missions are not quite ‘soft enough’ to detect a corona which can still be seen in EUV emission (energies  $\lesssim 0.2$  keV), routinely seen for decades in the solar corona in lines such as of Fe IX near 17 nm ( $\equiv 0.06$  keV).

This stellar sample includes only stars with fundamental characteristics demonstrably similar to the Sun (Egeland 2017). Figure 5 shows  $\mathcal{F}_{UV}$  against  $\mathcal{F}_{HK}$  for the sample, roughly following well-known non-linear relationships found for very diverse samples of stars (Oranje 1986; Oranje & Zwaan 1985; Schrijver et al. 1985; Schrijver 1995). But these linear fits in the log-log plane are not justified any more than, for example, a step function between the two groups of stars. It is adopted below merely to re-examine the power laws analyzed in the above cited work.

These data point to one conclusion: *the level of non-radiative heating, reflected in transition-region lines, converges to a level that is constant to within  $\pm 10\%$ , for G2 main-sequence stars older than  $\approx 2 - 4$  Gyr.*

### 2.5. The Sun as a star and its center-to-limb behavior

No high resolution ( $R \geq 10^4$ ) solar irradiance spectra exist, so we must compare stellar data with solar data from individual features on the Sun. Figure 6 shows

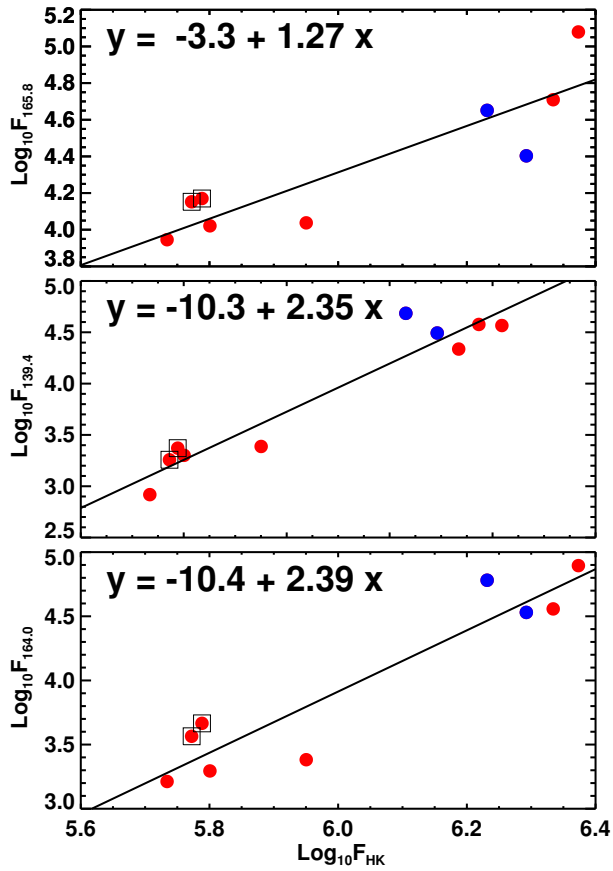


**Figure 5.** Scatter plots of surface flux densities  $\mathcal{F}$  for stars from 0.2 to 7.6 Gyr ages. The upper panel shows the C I 165.7 nm multiplet plotted against  $\mathcal{F}_{\text{HK}}$ , the lower the 139.3 nm line of Si IV and the 164.0 nm ( $B\alpha$ ) multiplet of He II. The latter is somewhat sensitive to coronal irradiation. As for Figure 4, the red dots show data from HST, the blue dots show (noisier) data from the IUE satellite. As in Figure 4, the error bars are smaller than the symbols.

spectral lines from the G130M flux spectrum of 18 Sco (there is to date no G160M spectrum) and  $\pi I_{\lambda}(\mu = 1)$  where  $I_{\lambda}(\mu = 1)$  is the quiet Sun intensity spectrum at disk center, at wavelength  $\lambda$ , which we adopt from the atlas of [Curd et al. \(2001\)](#). Here  $\mu$  is the usual cosine of the angle between the local vertical on the Sun and the line-of-sight to the observer. The assumption of no limb brightening/darkening – a Lambert radiator – is certainly incorrect ([Dammasch et al. 1999](#); [Worden et al. 2001](#)). It is made here to enable us to judge the departures from this approximation, and thereby understand results in the literature that appear to confuse flux-flux with intensity-intensity relations, which cannot be the same (see below). Assuming spherical symmetry, the

flux density  $f_{\lambda}$  observed a distance  $d$  from a star is:

$$f_{\lambda} = \frac{R_{*}^2}{d^2} 2\pi \int_0^1 I_{\lambda}(\mu) \mu d\mu, \quad (1)$$

where  $I_{\lambda}(\mu)$  is the outward directed intensity just above the stellar surface. The surface flux densities used above are simply  $\mathcal{F}_{\lambda} = f_{\lambda} \frac{d^2}{R_{*}^2} = f_{\lambda} 1.70 \times 10^{17} / \phi'^2$ . “Flat” limb behavior means  $I_{\lambda}(\mu)$  is independent of  $\mu$ ,  $\bar{I}_{\lambda}$ , so that

$$f_{\lambda} = \frac{R_{*}^2}{d^2} \pi \bar{I}_{\lambda} \quad (2)$$

Following [Judge et al. \(2004\)](#) we write departures from this “flat” limb behavior in terms of  $\beta_{\lambda}$ :

$$f_{\lambda} = \frac{\pi R_{*}^2}{d^2} I_{\lambda}(\mu = 1) \beta_{\lambda}, \quad (3)$$

where  $\beta_{\lambda}$  is given by

$$I_{\lambda}(\mu = 1) \beta_{\lambda} = 2 \int_0^1 I_{\lambda}(\mu) \mu d\mu. \quad (4)$$

Each individual wavelength  $\lambda$  has its own center-to-limb curve leading to its own  $\beta_{\lambda}$ . But it is possible to define a center-limb curve for an entire transition labeled  $i$ , in the case of optically thin lines and for narrow ranges of continuum wavelengths. [Judge et al. \(2004\)](#) list quantities  $\beta_i$  for the UV continuum below the edge of Si I at 152 nm, and wavelength-integrated emission lines, from various sources. Typically,  $\beta_i$  varies from close to 1 for continuum and optically thick transitions formed in the chromosphere, to 2.1 for thinner transitions formed in the less opaque transition region lines. The large differences between 18 Sco and the solar spectrum  $\pi I_{\lambda}(\mu = 1)$  evident in Figure 6 are at least partly attributable to these center-to-limb effects<sup>2</sup>. It is likely that remaining systematic differences between the 18 Sco and estimated solar flux spectrum exist because SUMER spectrum contains absolutely no active regions at all (Figure 2 of [Curd et al. 2001](#)), and spotless days are quite rare on the Sun. This, in spite of the fact that the COS spectrum of 18 Sco was observed in February of 2011, when the  $S$ -index of the star was measured to be at a minimum on decadal time scales, some 10% lower than typical values.

Within statistical uncertainties, we conclude that *the UV flux spectrum of 18 Sco is a useful proxy for the Sun-as-a-star*. It is a pity that no high quality Sun-as-a-star spectrum in the commonly observed vacuum UV region has been obtained.

<sup>2</sup> The data near 121.8 nm in Figure 6 shows another emission line in the L $\alpha$  wing, which is one of the two resonance lines of Mg X at 60.9794 nm, seen in SUMER’s second spectral order, absent in stellar spectra.



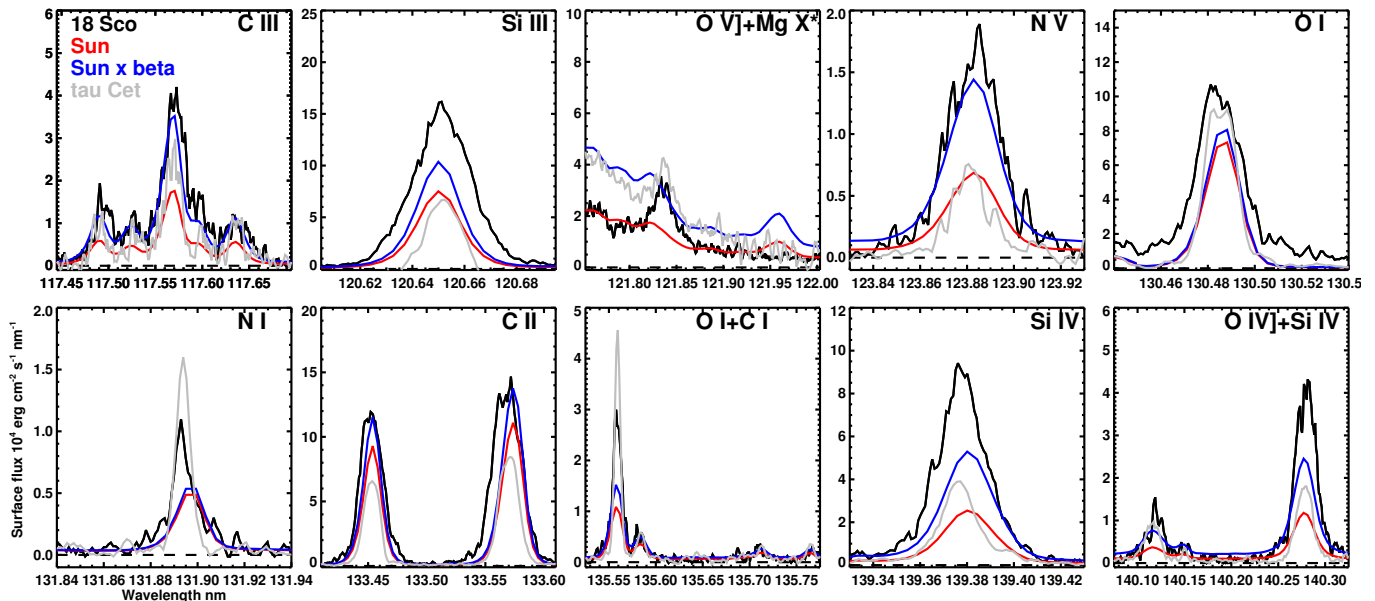


**Figure 6.** Flux densities  $\mathcal{F}_\lambda$  of 18 Sco are shown with disk-center data for the quiet Sun. The disk center intensity has been multiplied by  $\pi$  to produce a solar flux spectrum that assumes zero limb-darkening or brightening (red lines). The blue lines have been multiplied by the additional limb-brightening factors  $\beta_1$  discussed in the text.

### 2.6. De-convolution and detailed analysis of line profiles

The COS instrument has a “line spread function” (LSF) with a well-documented core-halo structure (Ghavamian et al. 2009). Considering only the core component, the COS instrument’s spectral resolution is  $R \approx 25,000$  ( $\equiv 12 \text{ km s}^{-1}$  in Doppler units). This resolution is more than sufficient to explore other signatures of magnetic activity that are present in the Sun and Sun-like stars. Wood et al. (1997) measured broad components of transition region lines in a wide variety of late-type stars, finding widths in the dwarf stars approaching  $10^2 \text{ km s}^{-1}$ , at the base of transition region lines. The only Sun-like stars in their sample are  $\alpha \text{ Cen A}$  and the Sun itself. In the Sun, these components result from “explosive events”, discovered with the HRTS instrument (Brueckner & Bartoe 1983; Dere et al. 1989; Dere 1994). Wood et al. (1997) found that in spectra of  $\alpha \text{ Cen A}$ , the broad components of lines of Si IV amounted to  $\approx 1/4$  of the total emission. In contrast, they estimated an upper limit of  $1/20$  for the Sun. Wood et al. (1997) were therefore hesitant to identify the  $\alpha \text{ Cen}$  profiles with explosive events. They termed the phenomenon microflares. As noted above, these authors had no choice but to compare stellar flux data with solar intensity data. With no knowledge of center-to-limb behavior of both components, this result is open to question.

Unfortunately, broad stellar components are qualitatively similar to the wings present in the LSF of COS.

But the LSF’s are very well known. De-convolution is therefore possible. Some additional “smoothness” constraint is needed to constrain the de-convolved profiles, because they are non-unique in the presence of noise. Assuming that the LSF’s are precise, we have de-convolved the COS spectra using the wavelength-dependent LSF’s appropriate for each wavelength region. We used the procedure `max_entropy.pro` released with the standard *SolarSoft* library to regularize the inversions. The presence of noise in the spectra (signal-to-noise ratios are  $\lesssim 30$ ) enforces some subjectivity in the application of such algorithms, as one must balance the regularization parameter (in this case the maximum permitted entropy of the recovered data) with the need to preserve spectral structure in the data. We found that 6 iterations of the algorithm were sufficient to provide a balance between these factors. The results are robust against different deconvolution parameters, including a maximum likelihood scheme.

The results are summarized in Figure 7. The upper panels show measured and deconvolved COS data as well as STIS data for  $\alpha \text{ Cen A}$ . The second and third rows show fits of double-Gaussian profiles and Voigt profiles to the deconvolved data. The data are shown for the Si IV line at  $139.3755 \text{ nm}$ , results for other lines are of lower quality owing to smaller S/N ratios, except for Si III which is probably affected by photon scattering.

The values of “chi<sup>2</sup>” listed in the figures, reduced- $\chi^2$  values, were derived from the noise reported by the HST software. The results as shown are clear. The STIS data

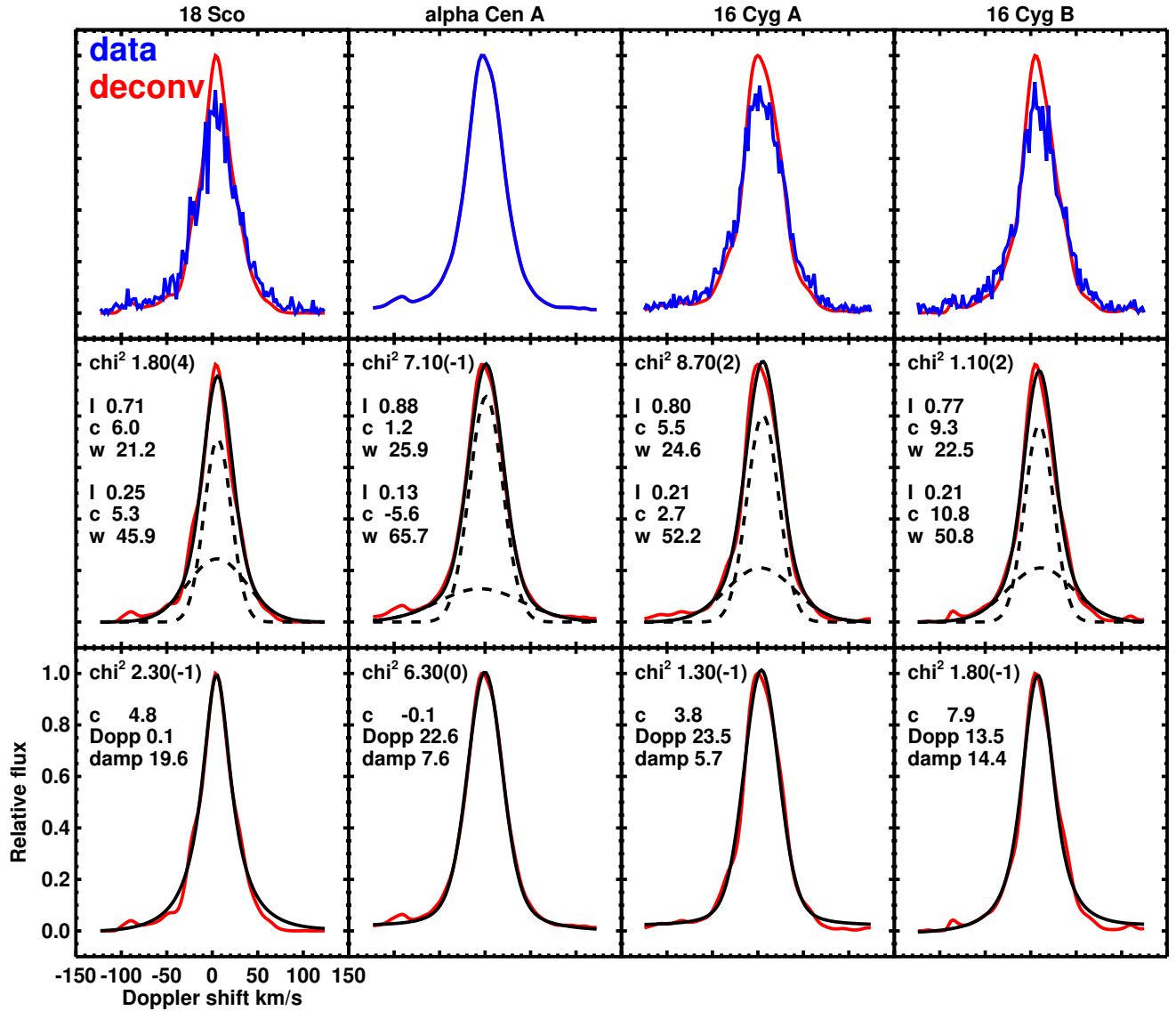


**Figure 7.** Raw and deconvolved profiles are shown in the upper panels, and fits to the deconvolved profiles are shown in the lower panels, for the 139.3755 nm line of Si IV. The data for  $\alpha$  Cen A are from the STIS instrument for which deconvolution is not necessary. “ $\chi^2$ ” is the reduced  $\chi^2$ , with notation 1.80(4)  $\equiv$   $1.80 \times 10^4$ . Two sets of values for the peak relative intensity  $I$  and line center  $c$  and width  $w$  are listed for the two Gaussian components in km/s, and Doppler and damping parameters are listed for the single Voigt component.

for  $\alpha$  Cen A shows clear evidence of Gaussian broad profiles as documented by Wood et al. (1997). The other stars for which only COS data are available, do not. 18 Sco, 16 Cyg A and B show profiles more consistent (according to  $\chi^2$  values) with Voigt than double-Gaussian profiles. Therefore we conclude that either: (1) the COS deconvolutions are simply too unreliable to be trusted, or (2) 18 Sco and the 16 Cyg stars genuinely show no detectable evidence of the “microflare” phenomenon reported by Wood et al. (1997).

Similar results (not shown) are found for the Si III 120.6 and Si IV 140.2 nm lines, in which the Voigt profiles are vastly superior to the double-Gaussian fits in every COS spectrum, except for  $\alpha$  Cen A, which reveals a broad component near 20 and 15% of the peak fluxes respectively. However, the derived values of the Voigt parameter ( $a = \gamma/4\pi\Delta\nu_D$ ,  $\gamma =$  damping width,  $\Delta\nu_D =$  Doppler width, both in frequency units) are much larger than can be accounted for by collisions or other physical effects in the emitting plasmas. ( $\gamma$  is given by “damp”

and  $\Delta\nu_D$  by Dopp in Figure 7). Perhaps residual instrumental effects are present even after the deconvolutions. The 120.6 nm line of Si III is significantly broader than the other stellar lines, suggesting some stellar opacity broadening in addition to Doppler motions, which may influence the interpretation.

On balance, it seems safe to conclude that HST spectra indicate the presence of microflare events in  $\alpha$  Cen A, but any phenomena comparable on 18 Sco, 16 Cyg A or B remain undetected. As a conservative upper limit, we can assume the broad components must have a peak brightness  $\leq 30\%$  of the narrow peak, simply by adopting the parameters of the double-Gaussian fits which have far higher reduced- $\chi^2$  values than their Voigt counterparts. The difference between the  $\alpha$  Cen A spectrum and disk spectra of solar explosive events remains unresolved, and will probably do so until genuine Sun-as-a-star measurements become available.

### 2.7. Unreasonable agreement?

The results highlighted in Figures 3 and 6 are, in a particular sense, worrisome. The measured flux densities of five Sun-like stars lie within 10% of one another, and the line profiles are remarkably similar. This result, initially gratifying, appears on deeper examination to be unsatisfactory, because of two related facts.

1. Well-known statistical correlations exist between fluxes of chromospheric ( $\mathcal{F}_{\text{ch}}$ ), and transition region and/or coronal lines ( $\mathcal{F}_z$ ) (Ayres et al. 1981; Oranje 1986). These take the form

$$\mathcal{F}_z = \mathcal{F}_{\text{ch}}^\gamma, \quad \gamma \geq 1. \quad (5)$$

These relations come from scatter plots of (mostly) single measurements of individual stars.

2. At the same time we also know that fluxes of chromospheric multiplets such as the Ca II *H* and *K* lines, vary significantly as a function of rotational and sunspot cycle phases (see Figure 2). For the Sun itself, the smoothed Ca II *S*-index varies from 0.162 at minimum to 0.177 (a change of +9%), with much larger excursions when including variability on shorter time-scales ( $\sim 0.156$ - $0.190$ , 22%; Egeland et al. 2017).

The problem is that if we differentiate equation (5), we find

$$\delta \ln \mathcal{F}_z = \gamma \delta \ln \mathcal{F}_{\text{ch}}. \quad (6)$$

Assuming that sampling an ensemble of stars is equivalent to seeing variations of a typical star (i.e., that equations 5 and 6 apply to each individual star), then *small fractional changes* in chromospheric emission ( $\delta \ln \mathcal{F}_{\text{ch}}$ )

should lead to *much larger fractional changes* in the corresponding fluxes in transition region and coronal lines ( $\delta \ln \mathcal{F}_z$ ). But the measured flux UV densities  $\mathcal{F}_{\text{UV}}$  of the five low-activity Sun-like stars lie within  $\pm 10\%$  ( $\pm 1\sigma$ ) of one another.

Let us assume (from the definition of *S*) that *S*-indices for such a homogeneous group of stars are linearly related to  $\mathcal{F}_{\text{ch}}$ , and for  $\mathcal{F}_z$  we use the Si IV 139.3 nm flux, because it has high S/N ratios. For this pair of lines the value of  $\gamma$  can be estimated from known logarithmic dependences of Mg II (chromospheric) and transition region lines, where (Oranje 1986),  $\gamma \approx 1.3$ . Using data from the F8 and G type dwarf stars in Table 2 of Oranje & Zwaan (1985) we would find that  $\mathcal{F}_{\text{Mg II}} \propto S_{\text{Ca II}}^{1.8}$ , where *S* is the “*S*-index”. Thus we expect that

$$\delta \ln \mathcal{F}_{\text{Si IV}} \approx 1.3 \times 1.8 \delta \ln S_{\text{Ca II}} = 2.4 \delta \ln S_{\text{Ca II}}. \quad (7)$$

Here we must only consider the non-linear relationship given by equation (5), without ad-hoc corrections for “basal” fluxes (e.g, Schrijver 1995). Note that equation (7), based upon previously published work, also applies roughly to our smaller sample with different ages, where  $\gamma \approx 2.35$  (Figure 5).

The LHS of equation (7) amounts to 10%, or 0.1 in  $\ln \mathcal{F}_z$ . To evaluate the RHS, we must estimate variations in *S*-index within each season’s observation that coincides with the epoch of UV observations. These amount to 2-4%. But, based upon high cadence solar observations, these values must be treated as strict lower limits since the time-series there are large gaps. Then, with  $\delta \ln S \gtrsim 0.04$ , we expect from (equation 6) that

$$\delta \ln \mathcal{F}_{\text{Si IV}} \gtrsim 0.1 \quad (8)$$

for each star. In pairwise comparisons of fluxes between stars, we must multiply by  $\sqrt{2}$ . Therefore we should observe (random) differences between the measured flux densities with an expectation variation of *at least* 14%. It is in this sense that *this agreement is perhaps unreasonable*.

Given the small numbers of stars and the single-epoch stellar UV observations, the disagreement cannot be considered statistically significant. However, in the Appendix we show how essential physics of the passage of active regions across stellar disks influence the interpretation of such data in the future. The new elements include the different geometry of formation of chromospheric and transition-region (and coronal) lines, and the very different center-limb variations of these features. These considerations have significant implications for “flux-flux” relations and “basal fluxes” (Schrijver 1995) as discussed below.

### 3. DISCUSSION

We have compared UV emission line spectra of Sun-like stars from age 0.2 to 7.6 Gyr. The first significant result is shown in Figure 2, namely that for stars of solar mass (excluding  $\tau$  Ceti) the median S indices seem to drop with age. Equally significant though is the observation that the variances in S index fall with age, in the latter half of the main sequence.

In contrast, our UV observations, mostly from one observation of each star, show that the bright cores of emission line profiles are remarkably similar for all the  $> 4$  Gyr G2-G3 stars studied here, independent of age, and measurably different from  $\tau$  Ceti (Judge et al. 2004). We have suggested an explanation for why such similar core UV profiles exist, given the statistical power-law relationships between UV and Ca II flux densities, and random sampling from measured variations of Ca II.

The broad components of the transition region lines examined in  $\alpha$  Cen A by Wood et al. (1997), confirmed here, are not present in the COS spectra of 18 Sco and 16 Cyg A and B, as judged by the far smaller  $\chi^2$  goodness-of-fit measures for Voigt, not double-Gaussian, profiles. Interestingly, of the five stars under study,  $\alpha$  Cen A and  $\tau$  Ceti have the highest and lowest masses and radii. The data do not support the idea that broad components decay significantly in time from 4 Gyr to 7.6 Gyr, which would otherwise indicate that explosive events will become rarer as the Sun ages on the main-sequence. Although Voigt profiles provide quantitatively better fits than double Gaussian profiles that have been used previously (Wood et al. 1997; Peter 2000), the unphysically large Voigt parameters  $a \gtrsim 0.1$  seem to point to residual effects from the COS instrument, or (less likely) weak blended emission lines, improperly accounted for by the deconvolution. Higher quality data would be worth obtaining, including a first G160M spectrum of 18 Sco.

The origin of the significant spectral differences between  $\tau$  Ceti and the other stars cannot be identified uniquely.  $\tau$  Ceti has a lower mass, older age, and it may be seen almost pole-on (Judge et al. 2004). Previous work, based upon weak variations in S-index (Balunas et al. 1995), suggested that these spectra could reflect conditions present during a “Grand Minimum” episode Judge et al. (2004). But both 16 Cyg A and B have “flat” S-index activity records, with quite different spectra from those of  $\tau$  Ceti. These findings cast doubt on the proposal that flat activity in stars like  $\tau$  Ceti is really associated with a solar-like “grand minimum”.

The Sun typically exhibits 10-15% variations in chromospheric activity over its 11 year activity cycle (Ege-land et al. 2017). However, as shown by Ayres (2014, and references therein), the Sun’s coronal X-ray emis-

sion (0.2-2.5 keV) changes by 7-8 times over its activity cycle. For 16 at least Cyg A (and perhaps B), the X-ray emissions indicate that magnetic dynamos are still operating in these older suns. The very low  $L_X$  observed for 16 Cyg B might be explained if 16 Cyg B was observed near the minimum state of an X-ray coronal cycle, or a large magnetically unipolar region (coronal hole) might dominate the visible hemisphere of 16 Cyg B during the Chandra visit. We plan to request additional X-ray observations of the 16 Cyg system using the enhanced soft response of the Chandra HRC, to determine possible short (rotation driven) and long-term variations in coronal activity of 16 Cyg B and its companions.

A corollary of our work (in the Appendix) is that, when considering “flux-flux” relationships (Oranje 1986; Oranje & Zwaan 1985), one cannot mix spatially-resolved data for the *intensity* of spectral features with those of unresolved *fluxes* from stellar disks, as done by (Schrijver et al. 1985; Schrijver 1992, 1995) for example. This is most easily seen by considering the passage of one active region across the disk of the Sun or a star. The Ca II S-index, sampling a mix of chromospheric (core) and photospheric (wing) emission, forms under optically thick conditions in which limb darkening occurs (radiation is peaked in the radial direction). Lines such as Si IV form under much thinner conditions and are limb brightened. This means that the same active region will exhibit one ratio of  $I_{\text{Si IV}}/I_{\text{Ca II}}$  near the limb and another at disk center. The solar active region McMath 12488 analyzed by Schrijver et al. (1985); Schrijver (1992) sampled disk-center data only, with  $0.92 < \mu \leq 1$ . These data were used by Schrijver to draw intensity-intensity relationships on the same footing as flux-flux relationships. But the analysis is on shaky grounds, for if these analyses had been performed close to the solar limb, entirely different results would have been found, invalidating the entire approach (see the Appendix). The different center-to-limb-intensity variations translate into time-dependent rotational modulations in disk-integrated fluxes which are quite different, depending only on the (observer-dependent)  $\mu$ -angle of the active region.

The question arises as to the evolution of the broad features, perhaps analogous to solar explosive events, from 4 to 7 Gyr. There is no clear one-to-one correspondence with age in our data, since 18 Sco and 16 Cyg A and B (no detectable broad regions) and  $\alpha$  Cen A (20-25% broad region contribution) would indicate an increase and then decrease of broad emission features with age. As documented by Dere et al. (1989), solar explosive events seem to avoid active regions and peak at mid latitudes in association with the bright chro-

ospheric network where magnetic field is concentrated in quiet regions by supergranular advection. They are equally present in coronal holes as in quiet regions, indicating that the large-scale pattern of magnetic field is unimportant for the generation of such events. Later, [Dere et al. \(1991\)](#) “identified [explosive events] with magnetic reconnection that occurs during the cancellation of photospheric magnetic flux,” associated with small-scale emerging flux during the formation of active regions, as well as along supergranulation cell boundaries.

More data of higher quality appear necessary to probe the evolution of surface magnetism on main sequence Sun-like stars. The broad-line regions are important because they directly reflect magnetic processes occurring significantly above the sound speed in the emitting plasma.

#### 4. SUMMARY AND OUTLOOK

UV spectra of the main-sequence solar mass stars reflect the changing surface magnetic fields as a function of age. Even for stars of 7 Gyr age, the data reveal lines of four-times-ionized O V] and N V, which, outside of active region loops are powered via conduction of heat downwards from an overlying corona ([Jordan 1980, 1992](#)). The emerging picture is that while emerging magnetic flux and energy from beneath the surface decays rapidly with time up to between 1 and 2 Gyr ([Skumanich 1972](#); [Güdel 2007](#); [van Saders et al. 2016](#)), the magnetic energy re-radiated at UV wavelengths converges to a specific fraction of the star’s luminosity to within  $\approx 10\%$  after this age. Given the known variations of several tens of percent in UV line radiation with the solar cycle, this result was initially surprising, 18 Sco certainly supports a healthy magnetic activity cycle, yet the UV spectra are very similar to the non-cycling 16 Cygni stars. It is notable that the *S*-indices

of all stars at around the epochs of the UV observations are close to 0.16 to 0.17, suggesting that we have (by chance) obtained data close to minimum levels of activity of at least 18 Sco and  $\alpha$  Cen A. If this is the case, then our observations reflect the operation of a residual local and small scale, “turbulent” dynamo, in the presence of convective motions in a highly non-diffusive plasma (high magnetic Reynolds number), even in the absence of a large-scale dynamo driven in part by global stellar differential rotation (e.g. [Vögler & Schüssler 2007](#); [Lites 2011](#)). The presence of a large-scale variable magnetic field associated with decadal sunspot variations on the Sun is rare among G-type stars. Such cycling behavior is far more common among K stars on the main-sequence ([Egeland 2017](#)). Neither 16 Cyg A or B, with ages of 7 Gyr, exhibits cycling behavior in the *S*-index, yet their rotation periods are slightly smaller than for the Sun, and Rossby numbers very similar. This begs the questions: What causes cycling behavior in the first place? Will the future Sun exhibit current cycling behavior as it ages on the main-sequence?

Lastly, it seems important to obtain genuine spectra of the Sun-as-a-star with spectral resolutions in excess of  $10^4$ , in order to make use of the rich UV archives of high quality UV data obtained with the Hubble Space Telescope. Such work is currently being proposed (C. Kankelborg, P. Judge and colleagues).

#### Acknowledgments.

We are grateful to Manuel Güdel for very helpful comments on the manuscript.

*Facilities:* Hubble Space Telescope, Solar and Heliospheric Observatory, Mt. Wilson *H* and *K* survey data, Lowell Observatory Solar Stellar Spectrograph, SIMBAD, IUE observatory.

*Software:* IDL Solarsoft

#### REFERENCES

- Allen, C. W. 1973, *Astrophysical quantities* (Athlone Press, Univ. London)
- Athay, R. G., & White, O. R. 1978, *ApJ*, 226, 1135
- . 1979, *ApJ*, 229, 1147
- Ayres, T. R. 1997, *JGR*, 102, 1641
- . 2017, *ApJ*, 837, 14
- Ayres, T. R., Judge, P. G., Saar, S. H., & Schmitt, J. H. M. M. 2008, 678, L121
- Ayres, T. R., Marstad, N., & Linsky, J. L. 1981, *ApJ*, 247, 545
- Baliunas, S., Sokoloff, D., & Soon, W. 1996, *ApJL*, 457, L99
- Baliunas, S. L., Donahue, R. A., Soon, W. H., et al. 1995, *ApJ*, 438, 269
- Bazot, M., Christensen-Dalsgaard, J., Gizon, L., & Benomar, O. 2016, *MNRAS*, 460, 1254
- Bazot, M., Ireland, M. J., Huber, D., et al. 2011, *A&A*, 526, L4
- Brueckner, G. E., & Bartoe, J.-D. 1983, *ApJ*, 272, 329
- Buldgen, G., Reese, D. R., & Dupret, M. A. 2016, *A&A*, 585, A109
- Chapman, S. 1931, Proceedings of the Royal Society of London Series A, 132



- Curdt, W., Brekke, P., Feldman, U., et al. 2001, *A&A*, 375, 591
- Dammasch, I. E., Wilhelm, K., Curdt, W., & Schuehle, U. 1999, in *Magnetic Fields and Solar Processes*, ESA SP-448, 1165
- Davies, G. R., Chaplin, W. J., Farr, W. M., et al. 2015, *MNRAS*, 446, 2959
- Dere, K. P. 1994, *Adv. Space Res.*, 14, 13
- Dere, K. P., Bartoe, J.-D. F., & Brueckner, G. E. 1989, *Sol. Phys.*, 123, 41
- Dere, K. P., Bartoe, J.-D. F., Brueckner, G. E., Ewing, J., & Lund, P. 1991, *JGR*, 96, 9399
- DeWarf, L. E., Guinan, E. F., Engle, S. G., Robertson, J. A., & DePasquale, J. M. 2012, in *American Astronomical Society Meeting Abstracts*, Vol. 219, American Astronomical Society Meeting Abstracts #219, 152.18
- Drake, S. A., Singh, K. P., White, N. E., Mewe, R., & Kaastra, J. S. 1996, in *Astronomical Society of the Pacific Conference Series*, Vol. 109, *Cool Stars, Stellar Systems, and the Sun*, ed. R. Pallavicini & A. K. Dupree, 263
- Eddy, J. A. 2009, *The Sun, the Earth and Near-Earth Space: A Guide to the Sun-Earth System* (NASA)
- Egeland, R. 2017, PhD thesis, Montana State University
- Egeland, R., Soon, W., Baliunas, S., et al. 2017, *ApJ*, 835, 25
- Gaidos, E. J., Henry, G. W., & Henry, S. M. 2000, *AJ*, 120, 1006
- Ghavamian, P., Aloisi, A., Lennon, D., et al. 2009, *Preliminary Characterization of the Post-Launch Line Spread Function of COS*, Tech. rep.
- González-Riestra, R., Cassatella, A., & Wamsteker, W. 2001, *A&A*, 373, 730
- Güdel, M. 2007, *Living Reviews in Solar Physics*, 4, 3
- Guinan, E. F., Ribas, I., & Harper, G. M. 2003, *ApJ*, 594, 561
- Hall, J. C., Henry, G. W., Lockwood, G. W., Skiff, B. A., & Saar, S. H. 2009, *AJ*, 138, 312
- Hall, J. C., & Lockwood, G. W. 2004, *ApJL*, 614, 942
- Hall, J. C., Lockwood, G. W., & Skiff, B. A. 2007, *AJ*, 133, 862
- Houdek, G., & Gough, D. O. 2011, *MNRAS*, 418, 1217
- Jordan, C. 1980, *A&A*, 86, 355
- Jordan, C. 1992, *Memorie della Societa Astronomica Italiana*, 63, 605
- Judge, P. G. 2017, in *The 2013 IAC Winterschool on Cosmic Magnetic Fields* (Cambridge University)
- Judge, P. G., Carlsson, M., & Stein, R. 2003a, *ApJ*, 597, 1158
- Judge, P. G., Saar, S., Ayres, T. R., & Carlsson, M. 2004, *ApJ*, 609, 392
- Judge, P. G., Solomon, S., & Ayres, T. R. 2003b, *ApJ*, 593, 534
- Kervella, P., Thévenin, F., Ségransan, D., et al. 2003, *A&A*, 404, 1087
- Laming, J. M., & Feldman, U. 1993, *ApJ*, 403, 434
- Leighton, R. B. 1959, *ApJ*, 130, 366
- Li, T. D., Bi, S. L., Liu, K., Tian, Z. J., & Shuai, G. Z. 2012, *A&A*, 546, A83
- Linsky, J. L., & Avrett, E. H. 1970, *PASP*, 82, 169
- Linsky, J. L., Bushinsky, R., Ayres, T., Fontenla, J., & France, K. 2012, *ApJ*, 745, 25
- Linsky, J. L., France, K., & Ayres, T. 2013, *ApJ*, 766, 69
- Lites, B. W. 2011, *ApJ*, 737, 52
- Mamajek, E. E., & Hillenbrand, L. A. 2008, *ApJ*, 687, 1264
- Metcalfe, T. S., Creevey, O. L., & Davies, G. R. 2015, *ApJL*, 811, L37
- Metcalfe, T. S., Egeland, R., & van Saders, J. 2016, *ApJL*, 826, L2
- Mewe, R., Kaastra, J. S., & Liedahl, D. A. 1995, *Legacy*, 6, 216
- Oranje, B. J. 1986, *A&A*, 154, 185
- Oranje, B. J., & Zwaan, C. 1985, *A&A*, 147, 265
- Pagano, M., Truitt, A., Young, P. A., & Shim, S.-H. 2015, *ApJ*, 803, 90
- Paresce, F. 1984, *Astr. J.*, 89, 1022
- Peter, H. 2000, *A&A*, 360, 761
- Petit, P., Dintrans, B., Solanki, S. K., et al. 2008, *MNRAS*, 388, 80
- Pietarila, A., & Judge, P. G. 2004, *ApJ*, 606, 1239
- Schmitt, J. H. M. M. 1997, *A&A*, 318, 215
- Schrijver, C. J. 1992, *A&A*, 258, 507
- . 1995, *A&ARv*, 6, 181
- Schrijver, C. J., Zwaan, C., Maxson, C. W., & Noyes, R. W. 1985, *A&A*, 149, 123
- Skumanich, A. 1972, *Astrophys. J.*, 171, 565
- Skumanich, A., Smythe, C., & Frazier, E. N. 1975, *ApJ*, 200, 747
- Tang, Y. K., & Gai, N. 2011, *A&A*, 526, A35
- Valenti, J. A., & Fischer, D. A. 2005, *ApJSS*, 159, 141
- van Saders, J. L., Ceillier, T., Metcalfe, T. S., et al. 2016, *Nature*, 529, 181
- Vaughan, A. H., Preston, G. W., & Wilson, O. C. 1978, *PASP*, 90, 267
- Vidotto, A. A., Gregory, S. G., Jardine, M., et al. 2014, *MNRAS*, 441, 2361
- Vögler, A., & Schüssler, M. 2007, *A&A*, 465, L43
- Wahlström, C., & Carlsson, M. 1994, *ApJ*, 433, 417

- White, T. R., Huber, D., Maestro, V., et al. 2013, MNRAS, 433, 1262
- Wilson, O. C. 1968, ApJ, 153, 221
- Wilson, O. C. 1976, ApJ, 205, 823
- Wood, B. E., Linsky, J. L., & Ayres, T. R. 1997, ApJ, 478, 745
- Woolley, R. D. V. R., & Allen, C. W. 1948, MNRAS, 108, 292
- Worden, J. R., Woods, T. N., & Bowman, K. W. 2001, ApJ, 560, 1020
- Wright, N. J., Drake, J. J., Mamajek, E. E., & Henry, G. W. 2011, [ApJ](#), 743, 48

## APPENDIX

## CENTER-TO-LIMB EFFECTS ON ROTATIONAL, CYCLIC MODULATION, AND FLUX-FLUX RELATIONSHIPS

The “disagreement” found in the text is resolved through consideration of center-limb variations as active regions cross the stellar disks. Let us consider Ca II for which  $\beta_i \approx 1$ , and Si IV which has  $\beta_i \approx 2.2$ , and the passage of one active region across the stellar disk. When  $\beta_i \leq 1$ , the spectral feature is flat or limb-darkened; when  $\beta_i > 1$ , it is limb-brightened, a value of  $\beta_i = 2$  implies that  $I_i(\mu) \propto \mu^{-1}$ . This behavior also corresponds to an optically thin plane-parallel atmosphere.

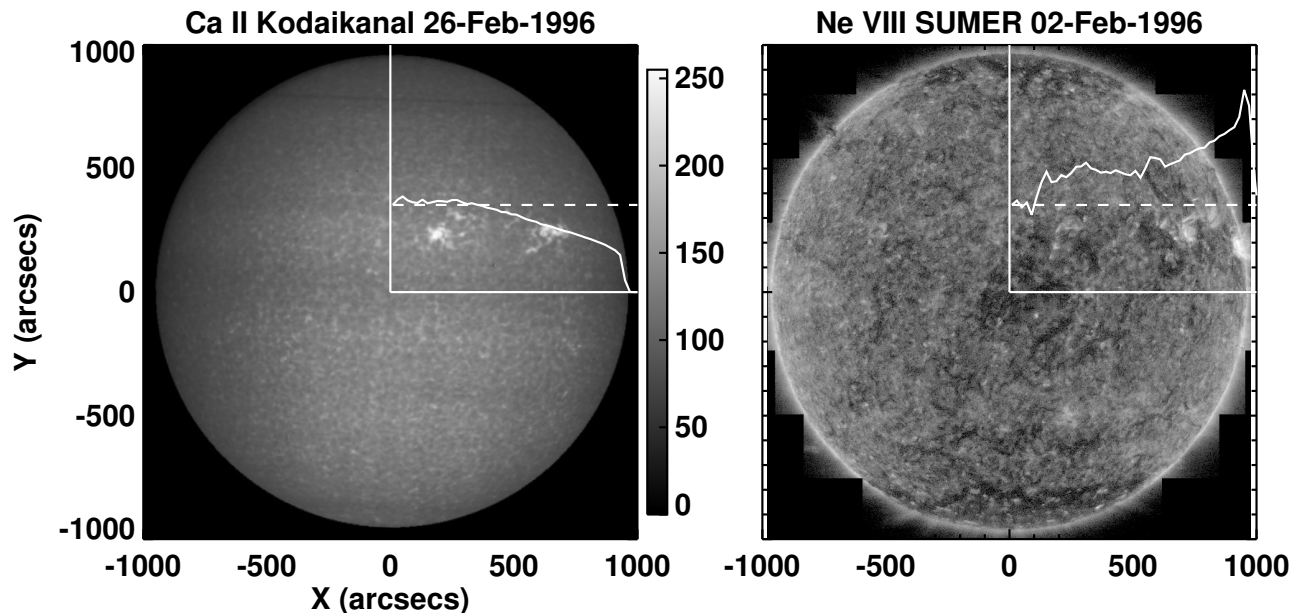


**Figure 8.** Intensity images are shown for the core and inner wings of the Ca II  $K$  line (from the Kodaikanal observatory archive) and in the Ne VIII coronal line from the SUMER instrument. The two images are from different days, during a very low activity period in February 1996. The line figures show the average center-to-limb behavior computed from the sector of quiet Sun between 7:30 and 10:30 on a clock-face. The dashed line shows no center-to-limb variation. The two curves are qualitatively different and the coronal line extends above the visible light limb.

As well as the background quiet Sun, We need to estimate the center-to-limb behavior of typical active regions. Unfortunately, active regions evolve significantly on time scales of a half-rotation, nor can we use existing (simultaneously measured) data from different vantage points in the solar system to determine center-limb behavior, because no imagers have obtained data for typical transition region lines<sup>3</sup>. Therefore we must use theoretical ideas to determine the C-L behavior of an active region.

The excess emission from chromospheric lines tends to form under optically thick conditions in plasma that lies within stratified layers of the atmosphere (Linsky & Avrett 1970). This is especially true at the wavelengths contributing to the  $S$ -index of Ca II  $H$  and  $K$ , where at least some of the emission passing through the  $S$ -index filter profile forms in the upper photosphere, in regions where there is a significant Wilson depression. The latter is important because radiation emerges from magnetic regions depressed below the average height. These conditions lead to  $\beta \leq 1$ . This means that the radiation is mostly *radially directed*, and the flux contributed by the AR is reduced by the fore-shortening of the

<sup>3</sup> The STEREO mission observes He II 30.4 nm emission. The problem is that helium lines are atypical (see, e.g. Pietarila & Judge 2004).

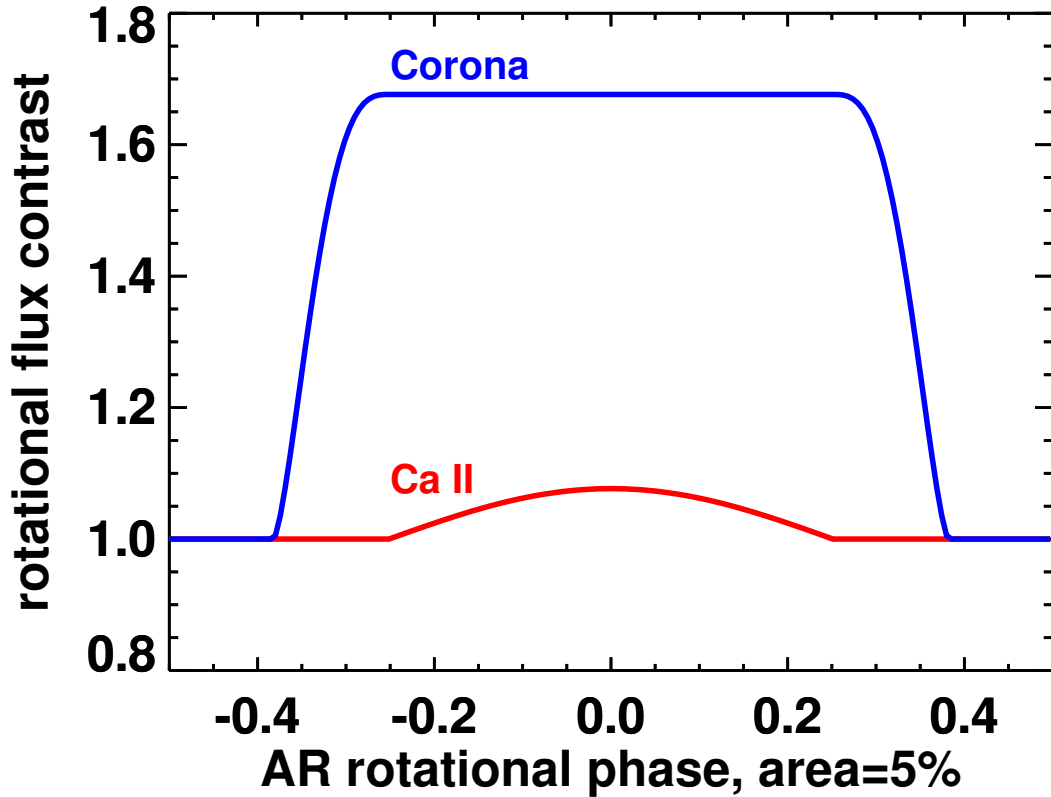


**Figure 9.** Computed rotational modulation of the total (disk-integrated) Ca II S index and optically thin coronal emission are shown as a function of rotational phase of an active region as it passes across a stellar disk. The background atmosphere is limb-darkened at Ca II wavelengths (using the parameters of Allen 1973) and limb-brightened, and extended across the limb by a pressure scale height (0.06 of the stellar radius) in the coronal bandpass. The active region covers 5% of the disk area, and is  $2\times$  (Ca II) and  $100\times$  (corona) brighter than the background disk-center intensity respectively. The disk-integrated Ca II has a 10% increase when the active region crosses central meridian. In spite of the small area and modest increase in brightness, the modulated signal in Ca II is 10%. The disk-integrated coronal modulation is just 70% in spite of the fact that the the AR is  $100\times$  brighter than the surrounding corona, because it adds to a strongly limb-brightened disk and emission from above the limb. Coronal AR emission is isotropic, once it transits the disk the flux is constant until it goes into eclipse.

projected area when close to the limb. As an active region crosses disk center, the contrast of the active region with its surroundings reaches a maximum.

In contrast, transition region and coronal lines form under far less thick conditions. In active regions, contributions to the coronal emission come from loops or from emission at the base of hotter loop structures. The same is true for transition region emission. The sum of all loop emission in an active region tends not to be fore-shortened and can be represented by the assumption of isotropic intensity. In contrast the foot-point emission can be fore-shortened ( $\text{area} \propto \mu$ ) and limb-brightened according to  $I(\mu) \propto \mu^{-1}$  if almost a plane-parallel emission region. In both cases the product of  $I(\mu)$  and the area contributing to flux is the same. Thus, in the limit of optically thin emission, the emission is isotropic, which leads to no center-to-limb variation (the emitting plasma overlying the active region emits the same power into all directions independent of heliocentric cosine  $\mu$ ). This is radically different from the thick (chromospheric) case, owing to both fore-shortening and limb darkening.

To illustrate these differences we show in Figure 9 the theoretical passage of an active region for one complete solar rotation, as it affects the total flux density  $\mathcal{F}$  for the thick and thin cases. The active region is assumed to be a disk (chromosphere) or sphere (for convenience, since for optically thin emission the geometry does not matter except very close to the limb), both covering 5% of the stellar surface. Phase zero is chosen to be when the active region is on

the central meridian. The chromospheric intensity contrast (active/quiet intensity at disk center) is set to a factor of two, the corona an enormous (!) factor of 100. (The exact numbers do not matter so long as the intensities follow non-linear relations of the kind measured for the Sun, e.g. [Schrijver 1992](#)).

The essential point of the figure is that the *modulations of integrated flux* (about 10% for Ca II, 68% for the “coronal” case) are *vastly different from the modulation of intensity*. When spatially resolved, the active region is only twice as bright in Ca II but is 100 $\times$  as bright in the “coronal” case! This figure therefore explains not only the “unreasonable agreement” in the main text, but has wider implications. The passages of active regions across disks of Sun-like stars are almost as easy to detect in limb-darkened transitions such as Ca II lines against a limb-darkened disk, as they are in thinner transitions in the corona and transition region. The latter show a far smaller flux contrast than the intensity contrast of the active regions. Along with previously noted problems concerning the energy sensitivities of various instruments ([Ayres 1997](#); [Judge et al. 2003b](#)), the calculations also explain the puzzle of why stellar activity cycles seen in fluxes of X-rays are of modest amplitude given the amplitudes in  $S$ -indices. This, in spite of the fact that solar active regions are so much intense in X-rays than quiet Sun.

Finally, the figure shows that more than 50% of the rotational phase space is filled with high flux contrast as optically thin emissions (“corona” in the figure) cross the disk. In comparison, the limb-darkened, fore-shortened thick flux contrast peaks with width in rotational phase a factor  $\geq$  two or more smaller. This means that in the presence of several active regions on the stellar disk, distributed in longitude, there is a higher probability that the “thin” cases will always have contributions from the active regions, potentially washing out the observability of flux modulation due to rotation compared with the “thick” cases.